buildings

MDPI

Article

Study on the Modification Method of Horizontal Additional Stress Under Strip Surcharge Considering Elastoplastic Characteristics of the Subgrade

Tao Chen [1], Guojiang Zheng [1], Chaoyi Sun [2], Bin Li [1], Nan Ge [1], Pengpeng Wang [2], Mingxing Zhu [2,*] and Zhengzhao Liang [3]

[1] Ningbo High-Grade Highway Construction Management Center, Ningbo 315000, China; 18868668911@163.com (T.C.); 13819834053@163.com (G.Z.); m17858936737@163.com (B.L.); genan604@163.com (N.G.)
[2] School of Civil Engineering and Construction, Jiangsu University of Science and Technology, Zhenjiang 212000, China; 241110901116@stu.just.edu.cn (C.S.); 13852720002@163.com (P.W.)
[3] State Key Laboratory of Coastal and Offshore Engineering, Dalian University of Technology, Dalian 116024, China; liangzz@dlut.edu.cn
* Correspondence: mxingzhu@just.edu.cn

Abstract

Aiming at the problem that strip surcharge in coastal soft soil foundations causes lateral squeezing and endangers the safety of adjacent existing bridge pile foundations, the traditional Boussinesq elastic theory cannot reflect the true elastoplastic characteristics of the soil and tends to underestimate the actual horizontal additional stress. This paper establishes a two-dimensional plane strain finite element model and, based on the calibration of pure elastic theoretical solutions, carries out extensive comparative analyses under elastoplastic foundation conditions. Through Pearson correlation and random forest sensitivity analyses, it is clarified that the internal friction angle, load ratio, and normalized distance ratio are the core control variables affecting the redistribution of horizontal additional stress, thereby demonstrating the limitations of the influence of elastic modulus and cohesion. The study reveals the nonlinear amplification mechanism of horizontal stress transfer caused by the penetration of the deep plastic zone within the foundation, as well as the physical evolution law of the stress correction factor, which initially exhibits a Gaussian peak enhancement and subsequently decays exponentially with spatial distance. Based on these mechanisms, a combined prediction formula for the horizontal additional stress correction factor is proposed, achieving an $R^2 = 0.903$, and a safety evaluation chart for the correction factor is constructed to quantify high-risk areas. The results indicate that when the normalized distance ratio is greater than or equal to 4, the elastoplastic squeezing effect essentially dissipates. The proposed modification method effectively delineates the applicable boundary of the elastic solution and provides a theoretical basis for the bearing capacity calculation and safety control of passively loaded pile foundations in soft soil regions.

Keywords: strip surcharge; induced horizontal stress; elastoplastic characteristics; correction factor; finite element analysis

Check for updates

Academic Editor: Eugeniusz Koda

Received: 20 May 2026
Revised: 20 June 2026
Accepted: 3 July 2026
Published: 5 July 2026

Copyright: © 2026 by the authors. Licensee MDPI, Basel, Switzerland. This article is an open access article distributed under the terms and conditions of the Creative Commons Attribution (CC BY) license.

1. Introduction

As a critical traffic lifeline in coastal areas, bridges play an irreplaceable role in regional economic development. However, with the continuous advancement of large-scale land

reclamation and urban construction in coastal areas, a series of complex geotechnical engineering hazards has inevitably been triggered. Among these, the issue of backfill or muck surcharge adjacent to existing bridge piles in soft soil foundations is particularly prominent. Surface additional surcharge disrupts the initial stress equilibrium of the soil, forcing highly compressible soft soil to undergo significant lateral squeezing deformation. This laterally displacing soil directly pushes against adjacent bridge pile foundations, forcing the piles into a passive loading state, which consequently leads to excessive bending deformation or even the risk of shear fracture, seriously threatening the safe operation of the bridges. In fact, pile foundation failures and engineering disasters caused by improper surcharge have been frequently reported both domestically and internationally. For example, based on field monitoring, Jones et al. [1] pointed out that the Surtees Bridge in the UK experienced significant post-construction lateral deformation of the soft foundation due to embankment backfill, and the massive lateral squeezing ultimately caused severe structural damage to the adjacent bridge pile foundations; Zhang Hao et al. [2], when analyzing the interaction mechanism between laterally displacing soft soil and passive piles, also emphasized that the core causes of many typical engineering disasters—such as the collapse of an industrial warehouse in Shanghai due to long-term surcharge and the "Lotus Riverside" building collapse incident—are closely related to the elastoplastic failure of the soil triggered by additional surcharge and the massive lateral thrust it exerts on adjacent pile foundations. Gu et al. [3] revealed the amplification effect of large-scale surcharge loading on the lateral deformation of passive piles and earth pressure in deep soft soil areas based on a three-dimensional numerical model; Zhou S et al. [4] systematically verified the significant spatiotemporal evolution characteristics of horizontal displacement and bending moment in adjacent bridge pile foundations under subgrade filling through centrifuge model tests. These painful engineering lessons fully demonstrate that accurately revealing the influence mechanism of surcharge on adjacent bridge pile foundations in soft soil has become an urgent engineering scientific problem to be solved.

There are two primary difficulties in researching the bearing characteristics of passive pile foundations under such surcharges: the first is the determination of the passive thrust on the pile body, for which Ito et al. [5,6] proposed a local plasticity theory to realize the conversion of horizontal additional stress into passive thrust on the pile foundation; the second is the calculation of the horizontal additional stress under surcharge, where domestic and international studies primarily rely on the Boussinesq elastic theory. In early research, Geber [7], Spangler [8], and Mindlin [9] analytically derived the distribution characteristics of lateral earth pressure on retaining structures under concentrated loads based on the principles of elasticity. Subsequently, Poulos and Davis [10] systematically reviewed and refined various elastic theoretical solutions in soil mechanics, laying a solid theoretical foundation for subsequent research. Within this theoretical framework, for different forms of surface surcharge such as strip loads and local point loads, engineering design manuals like NAVFAC [11] and numerous international scholars, including Steenfelt et al. [12,13], Georgiadis and Anagnostopoulos [14], Kim and Barker [15], and Iskander [16], further derived and simplified analytical or semi-analytical calculation methods for the lateral additional earth pressure behind retaining walls and sheet pile walls. As the engineering community's understanding of pile-soil interaction deepened, domestic scholars successively extended the application of these elastic theories to the passive loading analysis of single piles or pile groups. Wei Huanwei [17] and Li Fei [18] were among the first to conduct in-depth discussions on the lateral deformation effects of foundation and adjacent pile-soil systems caused by large-area ground surcharge and embankment fill based on Boussinesq solutions. To make the theoretical solutions better align with the actual pile-soil squeezing state in three-dimensional space, Zhu Mingxing et al. [19–21] creatively introduced the soil

arching effect in the calculation of horizontal additional earth stress. They not only derived semi-analytical solutions for the deformation and internal forces of passive piles under surcharge but also systematically revealed the bearing and anti-sliding mechanisms of passive piles and isolating piles under different surcharge modes. Deng Huiyuan [22] further comprehensively analyzed the evolution laws of pile bearing characteristics induced by surcharge, combining the complex foundation conditions of coastal hydraulic reclamation areas. Li Tingting and Yang Min [23] pointed out that under the combined action of overload and horizontal soil displacement, the lateral deformation of passive pile groups needs to be calculated and corrected by incorporating the theory of local plastic deformation. Wei Limin et al. [24] also emphasized that under large-area surcharge loading on deep soft soil, the additional horizontal stress exhibits a phased redistribution characteristic as the soil undergoes plastic flow. It is evident that the calculation of horizontal additional stress based on Boussinesq's theory has formed a mature analytical system, which also provides reliable stress boundary conditions for constructing more accurate theoretical calculation models for passive piles. However, the aforementioned studies are all based on the elastic theory system, which is approximately acceptable when the surcharge load is small or the foundation soil is of good quality. For soft soil foundations, however, there are significant application risks. The fundamental reason is that the elastoplastic characteristics of soft soil foundations differ vastly from an elastic system, which is also why engineering accidents involving bridge pile foundation failures under surcharge in soft soil areas occur frequently. Moreover, although previous works [17–24] have laid a solid foundation for passive pile loading, they often focused heavily on macro structural responses (moments/deflections) under specific case-by-case scenarios, heavily relying on custom FEA or complex empirical rules. A clear knowledge gap remains in defining a direct, generalized baseline for the horizontal stress field redistribution prior to pile formulation. This paper bridges this gap by decoupling the free-field horizontal additional stress correction factor (ξ) under strip distributed surcharges. This allows design engineers to instantly assess elastoplastic stress escalation boundaries directly from traditional Boussinesq solutions without invoking massive custom numerical operations.

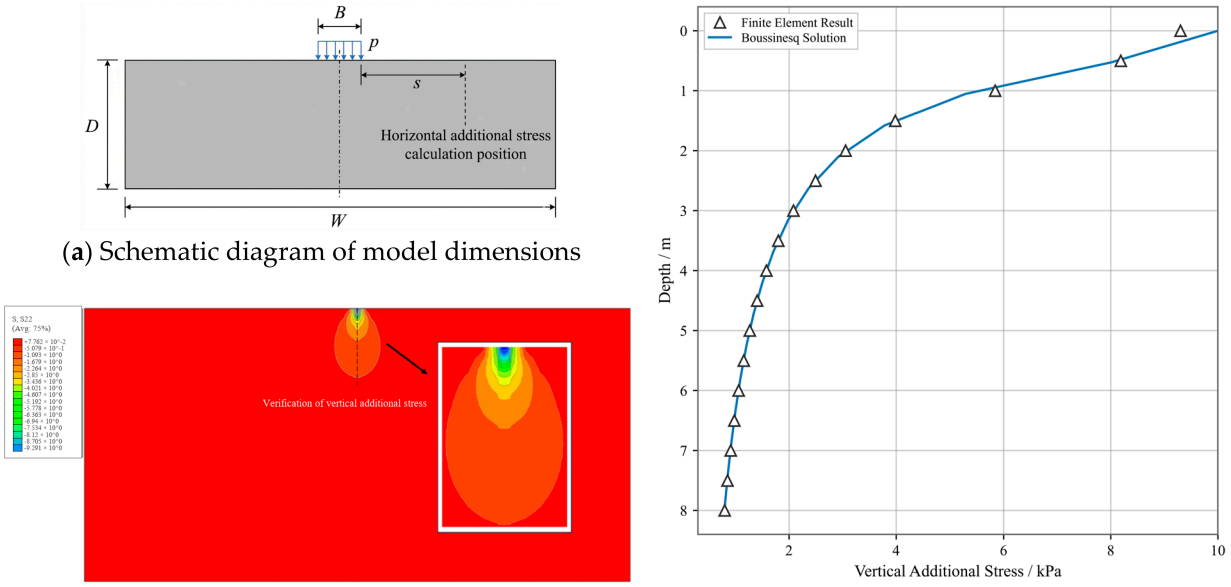
To resolve the uncertainty impact brought by the traditional elastic theory system's inability to account for the true elastoplastic deformation characteristics of foundations, this paper first establishes an elastic finite element model to calibrate with the elastic theory. Subsequently, considering the influence of factors such as foundation soil elastic modulus E, cohesion c, internal friction angle ϕ, distance ratio s/B, and foundation bearing capacity load ratio R, extensive comparative analyses of horizontal additional stress under strip distributed loads are conducted between elastic and elastoplastic finite element foundation models. This process extracts a calculation method for the horizontal additional stress correction factor ξ that accounts for the influence of the foundation's elastoplastic characteristics. As a fundamental methodological study, this research isolates pure mechanical mechanisms within a controlled continuum framework to establish a generalized baseline applicable to a broad range of geomaterials and foundation soils under strip surcharges, thereby focusing on rigorous theoretical verification against classical analytical solutions rather than site-specific empirical field reporting.

2. Verification of the Accuracy of the Finite Element Method for Elastic Theoretical Solutions

To avoid comparative errors caused by finite element discretization errors and the inability of theoretical analytical solutions to perfectly align in coordinate space, and to establish a rigorous theoretical benchmark for the subsequent elastoplastic analysis, this paper adopts the approach of directly comparing elastic and elastoplastic results within the

same finite element system. To ensure the reliability of this approach, the accuracy of the pure elastic finite element calculation results must first be verified.

This paper refers to a classic case in Sam Helwany's [25] book *Soil Mechanics with Abaqus*. As shown in Figure 1a, which represents the schematic diagram of the strip load model from Section 3.3.4 of the book, the strip load width is 1 m, the distributed load magnitude is 10 kPa, the elastic modulus E is 1×10^7 kPa, and the Poisson's ratio is 0.3. The plane strain model is 50 m high and 100 m wide. The boundary constraint conditions on the left side, right side, and bottom of the model are set to zero for both vertical and horizontal displacements (in the finite element model, $U_1 = 0$, $U_2 = 0$). The finite element mesh utilizes CPS4R elements, with a total of 2000 mesh elements. Because only the elastic model is considered, it is not necessary to set parameters such as unit weight or gravity, nor is it required to perform operations like geostatic stress balance.



(**a**) Schematic diagram of model dimensions

(**b**) Contour of vertical stress S22

(**c**) Comparison of vertical additional stress

Figure 1. Comparison of theoretical solutions with finite element vertical additional stresses: (**a**) Schematic diagram of model dimensions; (**b**) Contour of vertical stress S22; (**c**) Comparison of vertical additional stress.

The contour plot of the vertical additional stress S22 obtained from the finite element calculation is shown in Figure 1b. The results at a depth of 0–8 m directly beneath the center of the strip load distribution were selected for comparison, as illustrated in Figure 1c. The vertical additional stress solutions from the finite element calculation are essentially consistent with the theoretical solutions. Moreover, the results analyzed by the finite element method in this study align well with the case in Section 3.3.4 of *Soil Mechanics with Abaqus*. On one hand, this confirms the correctness of the finite element modeling and calculation process in this study. On the other hand, it demonstrates that the results of the finite element elastic model are nearly identical to the elastic theoretical solutions, allowing the finite element elastic model results to replace the theoretical solutions. This provides significant convenience for subsequent elastic-plastic solution comparison analysis.

The elastic solution of lateral additional stress compared with the finite element method is shown in Figure 2a. The results indicate that the outcomes of the finite element elastic model closely match the elastic theoretical solution, allowing the finite element elastic model results to replace the theoretical solution. Beyond this, this study further calculates the lateral additional stress at the edge of a strip distributed load. When the load increases to p = 100 kPa, the comparative results are presented in Figure 2b. Similarly, this further

demonstrates that the lateral additional stress results obtained from the finite element elastic model are essentially consistent with the Boussinesq elastic solution for lateral additional stress under strip distributed loads, proving the rationality and correctness of the finite element simulation.

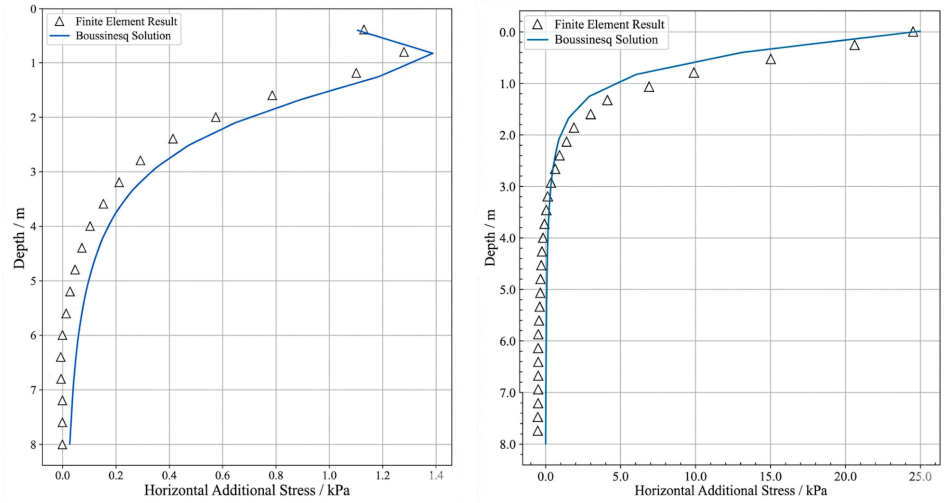


Figure 2. Comparison of theoretical solutions with finite element horizontal additional stresses: (**a**) case for p = 10 kPa; (**b**) case for p = 100 kPa.

The fitting results under the aforementioned multiple working conditions fully verify the correctness of the finite element modeling scheme, boundary condition constraints, and meshing adopted in this paper. The results also demonstrate that the pure elastic finite element model established in this paper can completely replace the theoretical analytical solution, which provides a reliable analytical baseline for the subsequent large-scale comparative analysis of additional stress modifications considering the elastoplastic characteristics of the foundation.

3. Study on the Modification Method for Horizontal Additional Stress Under Strip Surcharge

3.1. Establishment of the Finite Element Model

Road engineering is typically a linear engineering application; therefore, in subgrade analysis, the road load is often simplified as a strip distributed load. For the ABAQUS finite element simulation of strip distributed loads, a two-dimensional plane strain model is primarily adopted. This section needs to consider both elastic and elastoplastic models simultaneously. To control boundary effects, the model width must increase as the strip load width B increases. Combined with preliminary research, this paper sets the load width B = 4 m, the total model width W = 80 m, and the model height D = 40 m. To further improve computational efficiency, a symmetric model is utilized, as shown in Figure 3.

The finite element mesh adopts CPS4R elements, totaling 7006 units. The left and right boundaries of the model constrain horizontal displacement ($U_1 = 0$ in the FEM), and the bottom boundary constrains vertical and horizontal displacement ($U_1 = 0$, $U_2 = 0$). To facilitate batch analysis, the analysis steps for the elastic and elastoplastic models are set identically, as detailed below:

Step 1: The initial geostatic stress state of the subgrade is established based on the effective stress framework using Jaky's empirical formula $K_0 = 1 - \sin\phi$ to represent the long-term equilibrium before surcharge application. Subsequently, the external strip surcharge

is applied via a direct elastoplastic loading scheme, neglecting temporal consolidation to simulate the most critical operational phase immediately following rapid construction.

Step 2: The geostatic stress equilibrium step, selecting the Geostatic type and applying the gravity field.

Step 3: The application of the strip distributed load, choosing the Pressure method, noting that a positive value must be entered to represent downward pressure.

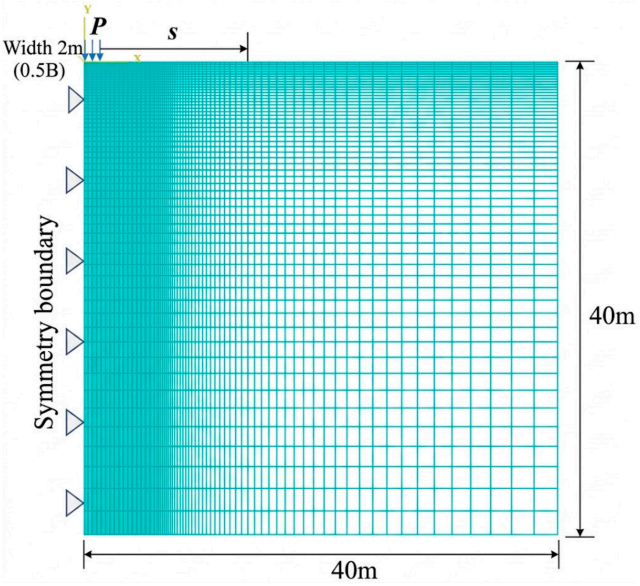


Figure 3. Finite element model of strip distributed load application.

The external surcharge is applied via a direct and immediate elastoplastic loading scheme under a standard initial K_0 state without temporal consolidation, which successfully encapsulates the peak lateral squeezing thrust to establish a conservative baseline for limit state design.

The elastoplastic model uniformly employs the Mohr-Coulomb constitutive model. Since the dilatancy angle in geotechnical materials is often much smaller than the friction angle ($\psi < \phi$), its physical behavior manifests as a non-associated flow rule, which forms an asymmetric stiffness matrix. Therefore, to ensure computational convergence, "Unsymmetric" is selected in the solver. The elastic model only requires deleting the "Mohr-Coulomb plasticity" material property item from the elastoplastic CAE model, keeping everything else unchanged to guarantee the accuracy of batch data processing. The finite element steps implement an immediate elastoplastic loading scheme under a standard initial K_0 state without consolidation, successfully capturing the peak lateral squeezing thrust for conservative limit state design. While critical-state models track micro-paths better, the Mohr-Coulomb model with a non-associated flow rule is utilized here due to its high parameter accessibility in routine geological records, balancing engineering practicality and macro stress boundaries. Crucially, the convergence and reliability of this identical mesh layout are verified via the analytical benchmarking in Section 2, where baseline stress fields achieve a near-perfect overlay with classical Boussinesq solutions. Consequently, the proposed method defines the upper bound of the induced horizontal stress field prior to long-term soil stabilization.

3.2. Calculation Parameters and Simulation Conditions

According to the Boussinesq elastic solution, the stress field is independent of the elastic modulus E and depends only on the load magnitude p and spatial position. However, when considering the elastoplastic characteristics of the soil, related parameters of the

Mohr-Coulomb model, such as cohesion c, internal friction angle ϕ, and the critical factor of foundation bearing capacity, must be taken into account. When the external load p is small, the foundation is in an elastic stage; as p increases, it gradually yields until complete failure.

This paper employs the Vesic formula as (1) to calculate the ultimate bearing capacity p_u [26].

$$p_u = cN_c s_c d_c i_c g_c b_c + qN_q s_q d_q i_q g_q b_q + \frac{1}{2}\gamma B N_\gamma s_\gamma d_\gamma i_\gamma g_\gamma b_\gamma \quad (1)$$

The expression for the bearing capacity coefficient in the above equation is as follows:

$$N_q = e^{\pi \tan \varphi} \tan^2\left(45^\circ + \frac{\varphi}{2}\right) \; N_c = (N_q - 1)\cot \varphi \; N_\gamma = 2(N_q + 1)\tan \varphi$$

The shape correction factor is (taking vertical load, horizontal ground, and horizontal base as examples):

$$s_c = 1 + \frac{N_q}{N_c}\frac{B}{L} \quad s_q = 1 + \frac{B}{L}\tan \varphi \quad s_\gamma = 1 - 0.4\frac{B}{L}$$

Referring to the typical parameter distribution ranges for soft to hard soils in the Engineering Foundation Handbook, to ensure the universality of the research conclusions, this paper selects a broad range of parameter variables, with specific values shown in Table 1.

Table 1. Range of finite element parameters.

No.	Parameter Variable	Value Range
1	Elastic Modulus E (MPa)	20, 40, 60
2	Internal Friction Angle ϕ (°)	15, 20, 25, 30, 40
3	Cohesion c (kPa)	5, 10, 20, 40
4	Load Ratio R (=p/p_u)	0.2, 0.4, 0.6, 0.7
5	Unit Weight γ (kN/m^3)	18.5 (Minimal fluctuation, approximated to mean)
6	Poisson's Ratio υ	0.35 (Minor fluctuation, standard value taken)
7	Distance Ratio s/B (Considered during results extraction)	0, 0.1, 0.25, 0.5, 1, 2, 3, 5, 7, 9

To balance analytical precision and computational efficiency, this paper uses orthogonal experimental design methods to combine the parameters in Table 1. An L25 orthogonal table (25 material combinations) is selected, and combined with 4 load ratio R levels, a total of 100 sets of finite element simulation conditions are generated for batch calculation. The ultimate bearing capacity p_u is calculated using the previously mentioned Vesic method, and combined with the load ratio R of the selected condition, the actual loading value p (=$R \times p_u$) in the model can be determined.

In addition, each model needs to extract horizontal additional stress data results when s/B is 0, 0.1, 0.25, 0.5, 1, 2, 3, 5, 7, and 9, respectively. Among them, the values extracted along the depth for each s/B are identically extended from the surface to 15 m underground. It should be noted that the extended parameter window with the friction angle reaching up to 40 degrees is intentionally adopted to capture the mechanical characteristics of heterogeneous coastal strata and composite or reinforced ground such as sand compaction piles and gravel columns, thereby enhancing the generalization capability of the formulation.

3.3. Sensitivity Analysis of Parameters

To avoid the overfitting caused by direct multivariable fitting, this paper utilizes Pearson and Spearman correlation coefficients as shown in Figure 4 combined with the random forest algorithm as shown in Figure 5 to conduct parameter sensitivity analysis on

the multivariate data obtained from finite element batch calculations, aiming to quantify the influence weight and direction of each parameter on the horizontal additional stress correction factor ξ.

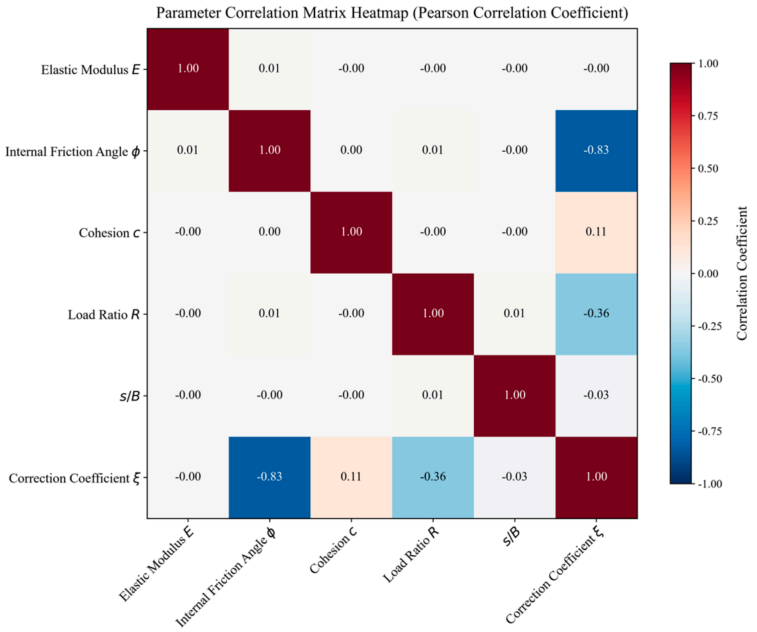


Figure 4. Parameter correlation matrix heatmap.

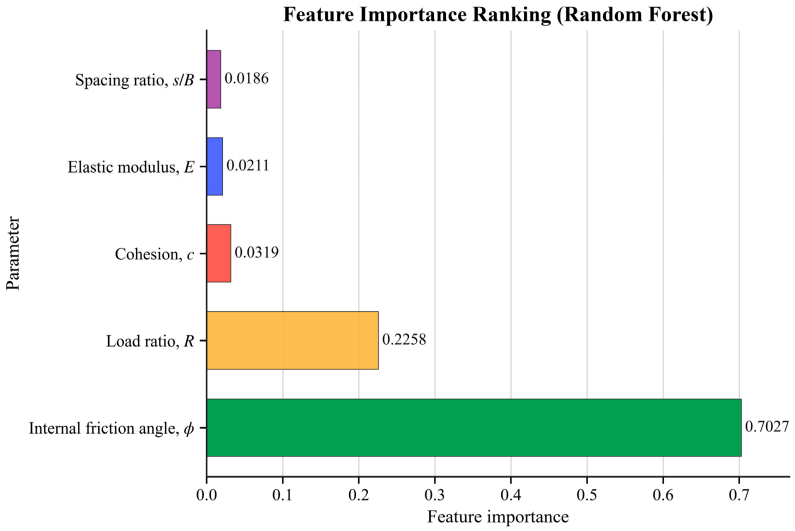


Figure 5. Random forest importance analysis.

Our goal is to establish a correction coefficient that takes into account multiple factors, as follows:

$$\xi = \xi(E, c, \varphi, R, s/B) \tag{2}$$

The comprehensive correlation analysis and random forest importance evaluation results indicate:

The internal friction angle ϕ is the core control factor affecting the correction factor. Its Pearson correlation coefficient reaches as high as -0.83, and its random forest feature importance is 0.7027, far exceeding other variables. From the physical mechanism analysis, ϕ determines the plastic flow boundary of the soil; the larger ϕ is, the stronger the nonlinear stress redistribution effect of the soil, leading to a significant decrease in ξ.

The load ratio R has a moderate intensity of influence. R is negatively correlated with ξ, with a Pearson coefficient of -0.36 and an importance of about 0.23, reflecting that the closer the load is to the ultimate bearing capacity of the foundation (i.e., the larger R is), the larger the plastic zone range, and the more the actual stress deviates from the elastic solution.

The distance ratio s/B exhibits a spatial attenuation effect. Although the overall correlation is weak, with an importance of 0.0186, the analysis shows that after s/B exceeds 3, ξ basically tends to stabilize and regress to 1, indicating that the correction factor has significant spatial limitations.

The influence of elastic modulus E and cohesion c can be ignored. The absolute value of the elastic modulus E is largely offset in the division format of the stress correction ratio ξ, with a correlation coefficient of only -0.0032; while the weak positive correlation of cohesion c, with an importance of 0.0319, has extremely limited practical correction significance for engineering applications.

In summary, to ensure the simplicity and generalization ability of the prediction formula, the influence of elastic modulus E and cohesion c should be eliminated. Ultimately, when constructing the prediction model for the correction factor ξ, it is only necessary to focus on three core independent variables: internal friction angle ϕ, load ratio R, and distance ratio s/B.

$$\xi = \xi(\varphi, R, \frac{S}{B}) \tag{3}$$

To ensure mathematical transparency and eliminate scale dependencies, the spatial and loading variables are inherently normalized into non-dimensional forms such as the distance ratio s/B and the load ratio R prior to the regression. This normalized representation ensures that the derived feature importance metrics faithfully reflect the intrinsic plastic yielding mechanisms of the soil domain under surcharges.

3.4. Horizontal Additional Stress Correction Factor

During the preliminary fitting of the global data for the horizontal additional stress correction factor ξ (distribution range ξ = 0.1~1.5), due to the large data span, the overall prediction accuracy of conventional single functions is low. Analyzing from the safety perspective in engineering practice, when $\xi \leq 1$, the horizontal additional stress under elastoplastic conditions is no greater than the value under elastic conditions; at this point, continuing to use the traditional Boussinesq elastic solution leans toward safety. However, when $\xi > 1$, the actual horizontal additional stress is underestimated, which constitutes a dangerous condition in engineering design. Therefore, the core purpose of establishing a prediction formula is to identify and quantify the high-risk regions where $\xi > 1$. To this end, this paper focuses on selecting the critical data interval of $\xi > 0.8$ for high-precision fitting modeling.

When constructing the prediction model, parameter sensitivity analysis indicates that the variation morphology of ξ presents significant non-monotonic characteristics. Because expressions of a single structural form struggle to accurately capture this peak mutation law, this paper proposes adopting a combined formula structure for fitting. Specifically, a Gaussian function is utilized to simulate the rapid peak effect in the initial stage, superimposed with the decay characteristics of an exponential function to describe the convergence process of the curve's tail toward ξ, as shown in Figure 6.

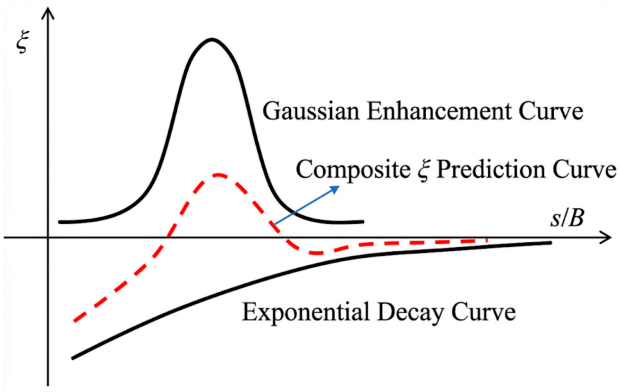


Figure 6. Schematic diagram of the prediction formula synthesis method.

The following formula can be obtained:

$$\xi = 1 + a \cdot \exp\left(-\frac{(S/B - \mu)^2}{2\sigma^2}\right) - d \cdot \exp\left(m \times \frac{S}{B}\right) \quad (4)$$

where a is the amplitude, μ is the relative position of the peak point, σ represents the relative width of the peak region, d represents the relative depth when the descending Gaussian curve crosses to $\xi = 1$, and m is the convergence coefficient of the tail of the curve.

Based on the above approach, a Python script was written to call the sklearn library to conduct global multiple regression analysis on a large amount of data, thereby obtaining the following prediction formula:

$$\xi = 1 + a(K_p, R) \cdot \exp\left(-\frac{(S/B - \mu(K_p, R))^2}{2\sigma(K_p)^2}\right) - d(K_p, R) \cdot \exp\left(-4.243 \times \frac{S}{B}\right) \quad (5)$$

where $K_p = \tan^2(45^\circ + \phi/2)$ is the passive earth pressure coefficient, and the expressions for each coefficient are as follows:

$$\begin{cases} a(K_p, R) = 0.432K_p^{1.5}R^{2.0} \\ \mu(K_p, R) = 0.572K_p^{0.4}R \\ \sigma(K_p) = 0.691K_p^{0.5} \\ d(K_p, R) = 0.171K_p^{1.8}R^{1.2} \end{cases}$$

The fitting accuracy verification is shown in Figure 7. The results indicate that the prediction formula for the horizontal additional stress correction factor ξ under strip distributed loads proposed in this paper achieves a coefficient of determination $R^2 = 0.903$ and a root mean square error RMSE = 0.0407. This model effectively avoids the discrete interference caused by global data and achieves high-precision prediction in the risk region of $\xi > 1$, which is highly emphasized in engineering, allowing it to be reliably used to evaluate the unsafety of traditional elastic solutions under specific conditions.

It should be noted that the proposed formulation (Equation (5)) functions as a semi-analytical empirical regression rather than a data-driven black-box prediction model. Since the 100 parametric cases are deterministically derived from verified, noise-free finite element simulations under a balanced orthogonal experimental design, a global regression analysis was performed on the entire dataset to maximize the statistical representativeness and robustness of the fitting parameters within the designated engineering domains. Furthermore, the extrapolation capability of the combined equation is physically validated by its asymptotic convergence to the classical Boussinesq solution (ξ~1.0) at far-field distances (s/B $\geq$ 4), eliminating the risks of numerical overfitting.

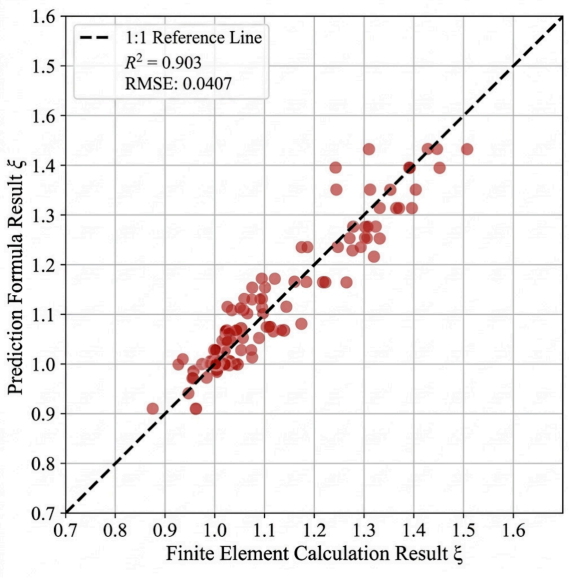


Figure 7. Comparison between predicted correction factors and finite element results.

4. Variable Influence Laws and Correction Factor Charts

4.1. Study on Variable Influence Laws

Figure 8 shows the comparative verification of the finite element calculation results under different working conditions utilizing the aforementioned prediction formula.

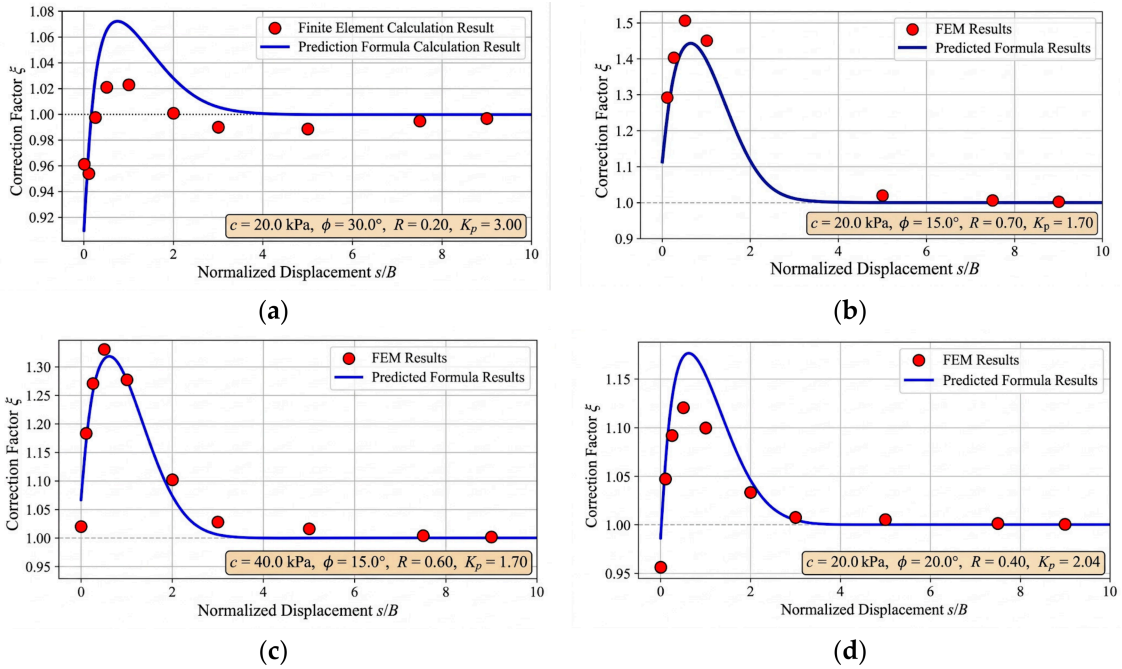
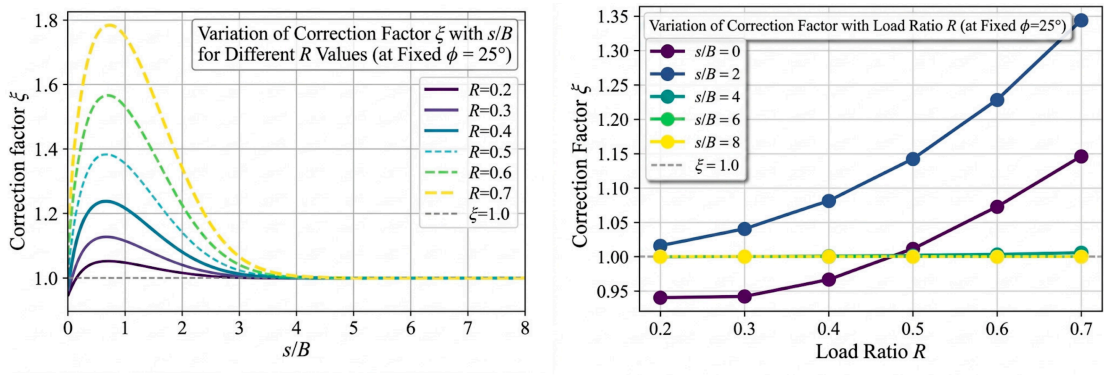


Figure 8. Comparison of predicted results and finite element calculation results under different working conditions: (**a**) comparison verification of condition 1; (**b**) comparison verification of condition 2; (**c**) comparison verification of condition 3; (**d**) comparison verification of condition 4.

From the above figures, it can be seen that the overall predictive effect of the prediction formula is excellent, capable of predicting and calculating the correction factor ξ under conditions with varying cohesion c, internal friction angles ϕ, and load ratio s R. More importantly, it can reliably capture the dangerous region where the correction factor $\xi > 1$. The above demonstrates that the prediction formula for the horizontal additional

stress correction factor under strip analysis loads established in this paper is reasonable and reliable.

Figure 9 illustrates the variation curve of the horizontal additional stress correction factor with s/B and load ratio R when the internal friction angle is fixed at $\phi = 25°$. As shown in Figure 9a, the variation law of the correction factor ξ with s/B is basically consistent with the morphology of the above prediction formula; it first undergoes a Gaussian enhancement phase, followed by an exponential decay phase. However, it can also be observed that basically when $s/B \geq 4$, the value of the correction factor ξ essentially tends to 1, meaning that when the distance from the edge of the strip-distributed load exceeds 4 times s/B, the elastic solution is consistent with the elastoplastic solution, and no further correction is needed. To further validate the physical soundness of the proposed elastoplastic correction factor ξ, a comparative analysis is conducted using the centrifuge test observations from Zhou et al. [4]. In their centrifuge tests regarding subgrade filling adjacent to passive piles, they noted that the lateral displacement and soil thrust did not decrease linearly with distance. Instead, a distinct nonlinear accumulation and squeezing zone occurred within a short distance near the loading edge (corresponding to s/B = 0.5 to 1.5 in this study), followed by a rapid dissipation of the squeezing effect as distance increased. This physical phenomenon perfectly corroborates the Gaussian peak enhancement and subsequent exponential decay of ξ discovered in this paper, proving that the pure elastic Boussinesq solution inherently under-predicts the high-risk squeezing stresses near the edge under actual plastic states.



(**a**) (**b**)

Figure 9. Variation pattern of correction factor when the internal friction angle is fixed at $\phi = 25°$: (**a**) the variation law of the horizontal additional stress correction coefficient with respect to s/B; (**b**) The variation law of the horizontal additional stress correction coefficient with the load ratio R.

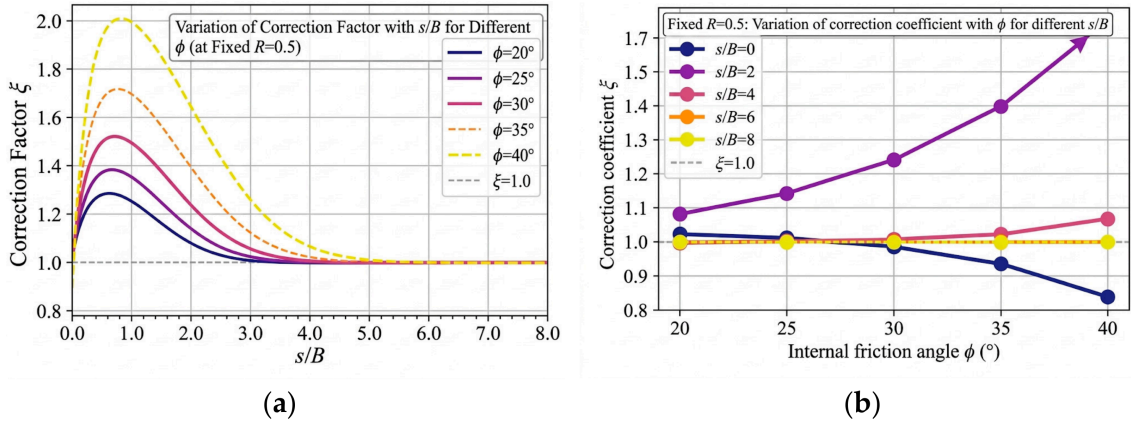
Simultaneously, it can also be seen that as the load ratio R increases, the curve exhibits an overall uplift and expansion, indicating that the higher the load intensity, the greater the horizontal additional stress value under elastoplastic conditions, and the area where it is greater than the elastic solution also gradually expands.

As shown in Figure 9b, it is evident that the correction factor ξ shows an increasing trend with the increase in the load ratio R. When s/B = 0 and 2, the increase amplitude of the correction factor ξ is relatively large; when $s/B \geq 4$, the value of the correction factor ξ basically does not change with variations in the load ratio R, which is consistent with the conclusion drawn from Figure 9a.

Figure 10 presents the variation curve of the horizontal additional stress correction factor with s/B and internal friction angle ϕ when the load ratio is R = 0.5.

As shown in Figure 10a, the variation law of the correction factor ξ with the internal friction angle ϕ is fundamentally consistent with the morphology of the prediction formula; it begins with a Gaussian enhancement phase, followed by an exponential decay phase.

However, it is also apparent that basically when $s/B \geq 4$, the correction factor ξ value essentially approaches 1, indicating that when the distance from the edge of the strip distributed load exceeds 4 times s/B, the elastic solution matches the elastoplastic solution, negating the need for further correction. As shown in Figure 10b, when $s/B = 0$, the correction factor ξ decreases as the internal friction angle ϕ increases; when $s/B = 2$~8, the correction factor ξ increases as the internal friction angle ϕ increases, though the rate of increase gradually diminishes. When $s/B \geq 4$, the correction factor ξ value basically remains unaffected by variations in the load ratio R, aligning with the conclusion from Figure 10a.



(**a**) (**b**)

Figure 10. Variation pattern of correction factor when the load ratio is fixed at R = 0.5: (**a**) The variation law of the horizontal additional stress correction coefficient with respect to s/B; (**b**) The variation law of the horizontal additional stress correction coefficient with the internal friction angle ϕ.

4.2. Correction Factor Chart and Its Significance

Figure 11 displays the horizontal additional stress correction factor ξ chart under strip distributed load. The solid line in this figure represents the boundary line of the correction factor $\xi = 1$; the area above this boundary line represents the region where the horizontal additional stress correction factor $\xi > 1$, and the area below represents the region where $\xi < 1$. This chart is generated by substituting the internal friction angle ϕ, load ratio R, and s/B values into the aforementioned prediction formula to calculate and identify the parameter combination space where the horizontal additional stress correction factor $\xi \geq 1$. An important function of this chart is the ability to quickly determine whether a coefficient correction for horizontal additional stress is necessary. For instance, if the chart indicates that the current engineering project is within a safe zone (the region where the correction factor $\xi < 1$), there is no need to consider the correction factor under elastoplastic influences. Otherwise, the correction factor value can be calculated according to the proposed prediction formula, thereby modifying the elastic solution.

It should be noted that the chart pattern when $s/B = 0$ is opposite to situations with other s/B values, which is consistent with the conclusion in Figure 10b. From the figure below, it can be seen that when $s/B = 0$, the safe zone is below the $s/B = 0$ boundary line, meaning the region where correction factor $\xi > 1$ is above it; whereas for $s/B = 1$~4, the safe zones are to the left of their respective boundary lines, meaning the region where correction factor $\xi > 1$ is to the right of their boundary lines. $s/B = 0.25$~0.5 belongs to the transition zone from 0 to 1; within this very short s/B range, the morphology of the correction factor chart undergoes a major transformation.

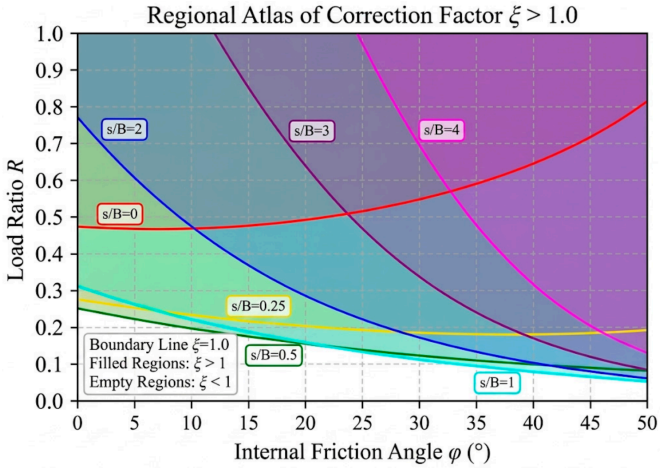
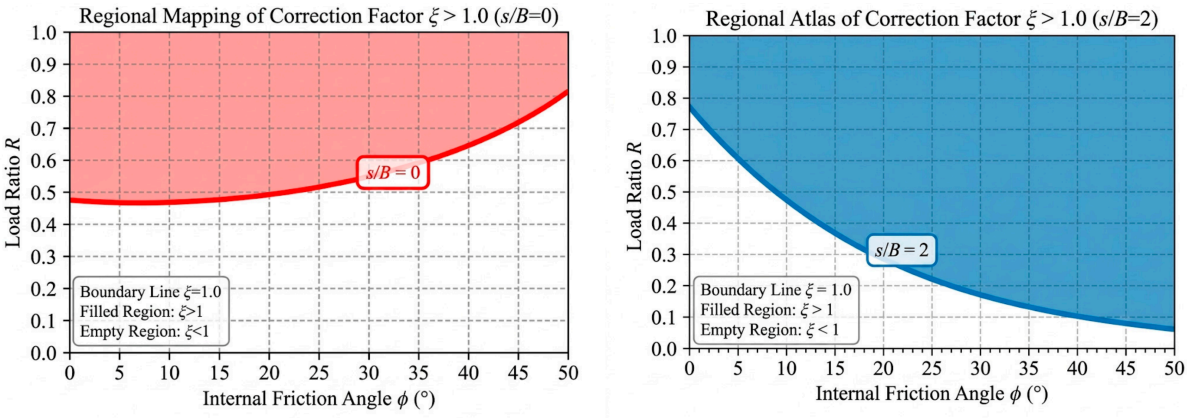


Figure 11. Diagram of correction factor ξ.

To further illustrate the meaning of the chart, the charts for $s/B = 0$ and $s/B = 2$ are extracted separately for explanation, as shown in Figure 12 below. As shown in Figure 12a, assuming a foundation bearing capacity safety factor of 2 during engineering design, the load ratio R = 0.5; from the figure, the corresponding internal friction angle $\phi = 20°$. This means that when the foundation soil maintains a constant $\phi = 20°$, if the actual subgrade load exceeds the design value (such as in cases of subgrade transport overload), the generated horizontal additional stress requires correction. Its connotation is that it proposes a demand value for soil strength enhancement, thus providing directional guidance for reinforcement and treatment. If the design load remains unchanged, but factors like soil consolidation cause the internal friction angle of the soil to increase, this is equivalent to increasing the safety reserve of the load.



(**a**) (**b**)

Figure 12. Application example of the correction factor ξ chart: (**a**) the graph when $s/B = 0$; (**b**) the graph when $s/B = 2$.

As shown in Figure 12b for the $s/B = 2$ chart, keeping the internal friction angle ϕ constant while increasing the load ratio R, or keeping the load ratio R constant while increasing the internal friction angle ϕ, will both cause the correction factor ξ value to fall into the $\xi > 1$ region, meaning the elastic horizontal additional stress value needs to be modified. Conversely, when $s/B = 0$, keeping the load ratio R constant and increasing the internal friction angle ϕ will cause the correction factor ξ value to drop into the $\xi < 1$ region.

5. Conclusions

Aiming at the calculation problem of horizontal additional stress caused by strip surcharge in coastal soft soil foundations, this paper established a two-dimensional plane strain finite element model, carried out comparative analyses of the mechanical characteristics of elastic and elastoplastic foundations, and proposed a horizontal additional stress modification method considering the elastoplastic characteristics of the foundation. The main conclusions are as follows:

(1) Traditional elastic theoretical solutions struggle to reflect the true elastoplastic characteristics of soft soil, and under high-risk engineering design conditions where the correction factor $\xi > 1$, they significantly underestimate the actual horizontal additional stress. Parameter sensitivity analysis shows that internal friction angle ϕ, load ratio R, and normalized distance ratios/B are the core control variables affecting horizontal additional stress redistribution, whereas the influence of elastic modulus E and cohesion c on the correction factor is extremely weak and is excluded from the calculations.

(2) The penetration of the deep plastic zone of the foundation possesses a nonlinear amplification mechanism on horizontal stress transfer. The horizontal additional stress correction factor ξ presents a non-monotonic evolution law along spatial distance: it initially shows Gaussian peak enhancement, followed by exponential decay. When the spatial distance reaches $s/B \geq 4$, the elastoplastic squeezing effect basically dissipates, and the correction factor ξ approaches 1.0, indicating that beyond this range, the classical Boussinesq elastic solution can be directly utilized.

(3) Based on the variable rules above, this paper proposes a combined prediction formula superimposing a Gaussian function and an exponential function. This formula has high prediction accuracy in the critical interval of $\xi > 1$, with $R^2 = 0.903$ and RMSE = 0.0407. The correction factor chart constructed based on this can intuitively define and quantify the boundary of dangerous areas requiring stress correction, providing a direct theoretical and quantitative basis for the bearing capacity calculation and safety treatment of passively loaded pile foundations in soft soil areas.

Author Contributions: Conceptualization, T.C.; Methodology, G.Z.; Software, B.L.; Validation, N.G.; Formal analysis, C.S., P.W. and M.Z.; Investigation, G.Z.; Resources, Z.L.; Data curation, T.C.; Writing—original draft, C.S.; Writing—review and editing, M.Z.; Visualization, N.G.; Supervision, B.L.; Project administration, Z.L.; Funding acquisition, P.W. All authors have read and agreed to the published version of the manuscript.

Funding: This work was supported by the Jiangsu Provincial Industry-University-Research Project (BY20251154) and the Ningbo Municipal Transportation Science and Technology Plan Project (202402).

Data Availability Statement: The data presented in this study are available in the article.

Acknowledgments: This work was supported by the Jiangsu Provincial Industry-University-Research Project (BY20251154) and the Ningbo Municipal Transportation Science and Technology Plan Project (202402). The authors are grateful for their support.

Conflicts of Interest: Authors Tao Chen, Guojiang Zheng, Bin Li and Nan Ge were employed by the company Ningbo High-Grade Highway Construction Management Center. The remaining authors declare that the research was conducted in the absence of any commercial or financial relationships that could be construed as a potential conflict of interest.

References

1. Jones, C.A.; Stewart, D.I.; Danilewicz, C.J. Bridge distress caused by approach embankment settlement. *Geotech. Eng.* **2008**, *161*, 63–74. [CrossRef]

2. Zhang, H.; Sun, K.; Yang, L.; Guo, Y. Passive pile-laterally moving soft soil interaction and passive load analysis of pile. *J. Civ. Eng. Manag.* **2020**, *37*, 45–51.
3. Yi, S.-C. Parametric study of passive piles subjected to adjacent surcharge load in extensively deep soft soil. *Front. Mater.* **2022**, *9*, 1080547. [CrossRef]
4. Zhou, S.; Feng, Z.; Liu, J.; Zhang, C.; Zhang, C.; Wang, J. Centrifugal model test study on the influence of subgrade filling on adjacent bridge pile foundations. *Buildings* **2025**, *15*, 4162. [CrossRef]
5. Ito, T.; Matsui, T. Methods to estimate lateral force acting on stabilizing piles. *Soils Found.* **1975**, *18*, 43–59. [CrossRef] [PubMed]
6. Ito, T.; Matsui, T. Extended design method for multi-row stabilizing piles against landslide. *Soils Found.* **1982**, *22*, 1–13. [CrossRef]
7. Geber, E. *Discussion of Investigations of the Distribution of Pressure in Locally Loaded Sand*; A.-G. Gebr. Leemann: Zurich, Switzerland, 1929.
8. Spangler, M.G. The distribution of normal pressure on a retaining wall due to a concentrated surface load. In *Proceedings of the International Conference on Soil Mechanics and Foundation Engineering*; Harvard University: Cambridge, MA, USA, 1936; pp. 200–207.
9. Mindlin, R.D. Discussion: Pressure distribution on retaining walls. In *Proceedings of the International Conference on Soil Mechanics and Foundation Engineering*; Harvard University: Cambridge, MA, USA; pp. 155–156.
10. Poulos, H.G.; Davis, E.H. *Elastic Solutions for Soil and Rock Mechanics*; John Wiley & Sons Inc.: Toronto, ON, Canada, 1974.
11. NAVFAC. *Foundations and Earth Structures*; United States Department of Navy, Naval Facilities Engineering Command: Washington, DC, USA, 1986.
12. Steenfelt, J.O.R.S.; Hansen, B. Discussion to "Total lateral surcharge pressure due to strip load" by Ramon Jarquio (October, 1981). *J. Geotech. Eng.* **1983**, *109*, 271–273. [CrossRef]
13. Steenfelt, J.O.R.S.; Hansen, B. Sheet pile design earth pressure for strip load. *J. Geotech. Eng.* **1984**, *110*, 976–986. [CrossRef]
14. Georgiadis, M.; Anagnostopoulos, C. Lateral pressure on sheet pile walls due to strip load. *J. Geotech. Geoenviron. Eng.* **1998**, *124*, 95–98. [CrossRef]
15. Kim, J.S.; Barker, R.M. Effect of live load surcharge on retaining walls and abutments. *J. Geotech. Geoenviron. Eng.* **2002**, *128*, 803–813. [CrossRef]
16. Iskander, G.M. Simplified analytical solution for point load acting behind a cantilever wall. *Int. J. Numer. Anal. Methods Geomech.* **2012**, *36*, 344–351. [CrossRef]
17. Wei, H. Study on the Influence of Ground Surcharge on Adjacent Pile Foundation. Master's Thesis, Tongji University, Shanghai, China, 2001.
18. Li, F. Study on Lateral Deformation Effect of Subgrade and Adjacent Pile-Soil Induced by Embankment Surcharge. Master's Thesis, Hohai University, Nanjing, China, 2005.
19. Zhu, M.; Gong, W.; He, X.; Xu, G. Semi-analytical solution for deformation and internal force of passive pile considering soil arching effect under surcharge. *Chin. J. Geotech. Eng.* **2013**, *35*, 1997–2008.
20. Zhu, M.X.; Gong, W.M.; Xu, G.P.; He, X.Y. Bearing mechanism analysis of axially loaded isolating pile under large-area surcharge. *Chin. J. Rock. Mech. Eng.* **2014**, *33*, 421–432.
21. Zhu, M. Study on Bearing Mechanism of Passive Pile Under Combined Load. Ph.D. Thesis, Southeast University, Nanjing, China, 2016.
22. Deng, H. Study on Bearing Characteristics of Pile Foundation Under Surcharge in Coastal Hydraulic Reclamation Area. Ph.D. Thesis, Southeast University, Nanjing, China, 2021.
23. Li, T.; Yang, M. Investigation of passive pile groups' responses induced by combined surcharge-induced and excavation-induced horizontal soil loading. *Buildings* **2023**, *13*, 2769. [CrossRef]
24. Li, S.; Wei, L.; Niu, J.; Deng, Z.; Wu, B.; Qian, W.; He, F. Time-dependent deviation of bridge pile foundations caused by adjacent large-area surcharge loads in soft soils and its preventive measures. *Front. Struct. Civ. Eng.* **2024**, *18*, 184–201. [CrossRef]
25. Helwany, S. *Applied Soil Mechanics with ABAQUS Applications*; John Wiley & Sons: Hoboken, NJ, USA, 2007. [CrossRef]
26. Salgado, R. *The Engineering of Foundations, Slopes and Retaining Structures*; CRC Press: Boca Raton, FL, USA, 2022.

Disclaimer/Publisher's Note: The statements, opinions and data contained in all publications are solely those of the individual author(s) and contributor(s) and not of MDPI and/or the editor(s). MDPI and/or the editor(s) disclaim responsibility for any injury to people or property resulting from any ideas, methods, instructions or products referred to in the content.